Title: Cold induces brain region-selective neuronal activity-dependent lipid metabolism

Authors: Hyeonyoung Min[1], Yale Y Yang[5], and Yunlei Yang[1,2,3,4*]

Affiliations:

1. Department of Medicine Division of Endocrinology, Albert Einstein College of Medicine, Bronx, NY, 10461, USA
2. Department of Neuroscience, Albert Einstein College of Medicine, Bronx, NY 10461, USA
3. Einstein-Mount Sinai Diabetes Research Center, Albert Einstein College of Medicine, Bronx, NY 10461, USA
4. The Fleischer Institute for Diabetes and Metabolism, Albert Einstein College of Medicine, Bronx, NY 10461, USA
5. Friends Seminary, New York, NY 10003, USA

*Correspondence author:

Yunlei Yang

Department of Medicine Division of Endocrinology

Department of Neuroscience

Albert Einstein College of Medicine

yunlei.yang@einsteinmed.edu

Tel: 718-430-8570

Abstract

Previous studies have been focused on lipid metabolism in peripheral tissues such as adipose tissues, while little or nothing is known about that in the brain. It is well recognized that cold acclimations enhance adipocyte functions, including white adipose tissue (WAT) lipid lipolysis and beiging, and brown adipose tissue (BAT) thermogenesis in mammals. However, it remains unclear whether and how the genes responsible for lipid metabolism in the brain are also under the control of cold acclimations. Here, we show that cold exposure predominantly increases the expressions of the genes encoding lipid lipolysis in the paraventricular nucleus of the hypothalamus (PVH). Mechanistically, we find that inactivation of neurons in the PVH blunts the cold-induced lipid peroxidation and lipolysis. Together, these findings indicate that lipid metabolism in the PVH is cold sensitive, potentially participating in cold regulations of energy metabolism.

Introduction

Lipid metabolism in peripheral tissues has been extensively studied, including white adipose tissue (WAT) lipolysis (*Grabner et al., 2021*) and beiging (*Bartelt and Heeren, 2014*) and brown adipose tissue (BAT) thermogenesis (*Carpentier et al., 2023*); however, an essential but poorly understood element is that of lipids in the central nervous system, particularly in the hypothalamus as it plays a crucial role in the regulation of systematic energy metabolism (*Waterson and Horvath, 2015*) and glucose homeostasis (*Pozo and Claret, 2018*). The brain is highly thermal sensitive in that one ^{o}C or less temperature changes can lead to functional alterations of the central nervous system (*Brooks, 1983; Wang et al., 2014*). Mounting evidence indicates that the brain is a metabolic organ that intensively produce heat (*Howarth et al., 2012; LaManna et al., 1980; Yablonskiy et al., 2000*), and brain temperature has recently increasingly drawn attention to both basic and clinical studies in normal and abnormal conditions, such as

stroke and neurodegenerative disorders. Lipids provide a major source of energy and heat in the body, however, the mechanism underlying brain lipid metabolism regulations remains a mystery. There is evidence to show that the brain's energy metabolism largely depends on the temperature (*Guyton and Hall, 2006; Yu et al., 2012*). In the brain, temperature gradients between different brain regions exist (*Anderson and Moser, 1995; Delgado and Hanai, 1966; Hayward and Baker, 1968; Mcelligott and Melzak, 1967; Moser and Mathiesen, 1996; Thornton, 2003*). We therefore assume that cold acclimations modulate brain lipid metabolism in temperature-sensitive brain regions that express the genes encoding lipid lipolytic and thermogenic enzymes. Identifying the brain regions and genes under the control of ambient temperature is thus crucial in both maintaining brain metabolism homeostasis and preventing fatty acid toxicity.

Here, we combine cold exposure, brain region-selective assays of gene expressions and lipid metabolic assays, and real-time fiber photometry monitoring of lipid metabolic activity *in vivo*, to define cold-sensitive brain region(s) and genes responsible for lipid metabolism in the hypothalamus and elucidate the involved mechanisms.

Results

Cold-induced brain region-selective gene expressions of lipolytic markers

To investigate a potential for cold exposure to modulate gene expressions for lipolysis and thermogenesis in the hypothalamus, mice were exposed to a cold (4 °C) chamber for 4 to 6 hours, a more physiologically relevant condition. Immediately after the cold challenge, mouse brains were acutely extracted and sectioned in ice-cold oxygenated artificial cerebrospinal fluids (ACSFs). Hypothalamic sections that respectively include PVH, lateral hypothalamus (LH), dorsomedial hypothalamus (DMH), ventromedial hypothalamus (VMH), and arcuate nucleus (ARC) were transferred to ACSF-containing incubators. Micro-punches of these brain

regions were subsequently made for gene assays of lipid metabolic markers.

To evaluate the effects of cold on the gene markers of lipolysis, we measured the mRNA levels of two key markers of lipolysis adipose triglyceride lipase (Atgl) and hormone sensitive lipase (Hsl). We observed that cold-challenged male mice showed a significant increase in the gene expressions of the Atgl (Fig. $1A_1$) and Hsl (Fig. $1A_2$) selectively in the PVH but not in other brain regions (Fig. 1B-E). We also assayed the gene expressions of thermogenic marker Ucp2 (Uncoupling protein 2) and additional thermogenic factors (Cidea, Prdm16). Cold did not significantly affect mRNA expressions of these thermogenic markers in all the examined regions in this study (Fig. 1). Meanwhile, we found that cold did not significantly affect gene expressions of these lipolytic and thermogenic markers in female mice (Supplementary Figure 1). These results suggest that cold exposure (4 ~ 6 h) could induce a rapid lipolytic activity to release fatty acids primarily in the PVH in males. Because cold did not significantly affect lipolytic markers in other regions and did not affect thermogenic markers, we next focused on studying cold-induced lipid mobilization and lipolysis in the PVH in males and elucidate the involved neuronal mechanisms.

Cold-induced formations of lipid droplets (LDs)

It is increasingly appreciated that lipid droplets (LDs), endoplasmic reticulum (ER)-derived intracellular neutral lipid storage dynamic organelles (*Olzmann and Carvalho, 2019*), are predominantly accumulated in adipose tissues and liver under normal physiological conditions (*Farese and Walther, 2009; Murphy, 2001*). Also, there is evidence to indicate that glial cells such as astrocytes and tanycytes in the brain accumulate LDs under metabolic and hypoxic stress (*Geller et al., 2019; Smolic et al., 2021*). A recent elegant study shows that hyperactive neurons release fatty acids from phospholipids to generate LDs in the brain and activation of neurons promotes lipolysis by increasing cytoplasmic lipases (*Ioannou et al, 2019*). These

findings suggest that increased neuronal activity and accumulated LDs probably contribute to the cold-induced increase in the lipolytic markers we observed in this study.

To probe the mechanism of the upregulation of lipolytic markers in the PVH, we evaluated the ability for cold to accumulate LDs. After the cold challenge, mouse brains were perfused, fixed, and sectioned. Hypothalamic sections containing the PVH were stained using the BODIPY 493 (BD493), a LD probe which has been widely applied to measure LD number and area in fixed tissues and live cells respectively (*Geller et al., 2019; Ioannou et al., 2019; Liu et al., 2015; Long et al., 2012; Smolic et al., 2020; Spangenburg et al., 2011*). Interestingly, we observed that a short-term (30 min ~ 1 h) cold exposure induced an increase in the LD area in the PVH (Fig. 2A-C). We verified LDs by using the cytoplasmic LD-binding protein perilipin-2 (Fig. 2D-F). However, a longer (4 ~ 6 h) cold exposure reduced the number of LDs (Supplementary Figure 2), which might be due to cold-induced liberations of fatty acids from the LDs to mitochondria for β-oxidation.

Cold increases Fos expressions in PVH

We next examined whether and how cold modified cell activities in the PVH *in vivo*. Mice were placed in a cold chamber before mouse brains were perfused and fixed. PVH sections (40 μm in thickness) were stained using anti-Fos antibodies. Mice subjected to the cold challenge showed increased expressions of the activity indicator Fos in the PVH as compared to control mice (Fig. 3A-C).

***In vivo* real-time photometry monitoring of cold-induced lipid peroxidation**

Lipid peroxidation is essential in neuronal activity-dependent LD formations (*Ionanna et al., 2019*), so we evaluated the capability for cold to induce lipid peroxidation. Fiber photometry has recently been applied to detect the levels of fluorescent biosensors *in vivo* by us (*Chen et*

al., 2022) and others (*Andersen et al., 2023; Sun et al., 2018*). To achieve this goal, we thus combined *in vivo* time-lapse two-color photometry monitoring and the BODIPY581/591 C11 (BD-C11) ratiometric lipid peroxidation sensor. We developed and validated an approach to simultaneously monitor both red and green signals in one brain region through an implanted photometry fiber connected to a two-color photometry system, for the BD-C11 sensor as it shifts its fluorescence emission peak from 590 (red) and 510 (green) nm when oxidized. A custom-made Optical fiber multiple Fluid injection Cannula (OmFC) implanted over the PVH was used for both BD-C11 injection and photometry monitoring of the two signals in freely behaving mice. Intra-PVH injection of the BD-C11 sensor through the OmFC was previously performed 4 h before placing the mice in a temperature-controlled chamber. Our photometry results show that cold potently increased the BD-C11 ratio (green to red), indicating cold-induced increase in lipid peroxidation (Fig. 4A). To further validate our photometry approach and the BD-C11 sensor, we treated mice with a lipid soluble antioxidant α-tocopherol (α-TP) to inhibit lipid peroxidation. Compared to vehicle-treated mice (Fig. 4B), we observed that prior inhibition of lipid peroxidation with the α-TP blunted the cold-induced effects (Fig. 4C). These results demonstrate that cold is capable to induce lipid peroxidation in the PVH, and that our combined photometry and BD-C11 approach can be reliably used to evaluate the dynamics of brain lipid peroxidation in a spatiotemporal manner.

Cold-induced lipid peroxidation is under the control of neuronal activity

We next sought to examine whether lipid peroxidation is under the control of neuronal activity. To define a role of neuronal activity in the cold-induced lipid peroxidation, we took advantage of the combined photometry system and BD-C11 system. To inhibit neuron activity, we applied the $GABA_A$ receptor agonist muscimol (MUS) (*Barbalho et al., 2009; Sanders and Shekhar, 1995*) and glutamate receptor antagonist Kynurenic acid (KYN) (*Yoshida et al., 2012*). To

verify the inhibitory effects of the combined chemicals, we performed intra-PVH injection of MUS and KYN in mice virally transduced with the protein of Ca^{2+} indicator $GCaMP_{6f}$ in the PVH (Supplementary Fig. 3A). Thirty min post the MUS and KYN administration, we performed time-lapse photometry monitoring of the $GCaMP_{6f}$ signals. We observed that MUS+KYN treatment significantly reduced the spikes of the $GCaMP_{6f}$ signals compared to controls (Supplementary Fig. 3B-C). This result demonstrates that the two combined chemicals can be used to inhibit neuronal activities *in vivo*. To test whether neuronal inactivation could diminish the cold-induced effect on lipid peroxidation, intra-PVH injections of MUS and KYN were performed 30 min before placing the previously BD-C11 injected mice in the chamber, and photometry monitoring of BD-C11 signals were then performed. MUS and KYN inactivation of neurons prevented the cold-induced increase in the BD-C11 ratio (Fig. 4D), indicating that cold-induced lipid peroxidation is under the control of neuronal activity.

Neuronal inactivation prevents cold-induced lipolysis

To evaluate lipolysis in the PVH, we performed intra-PVH injections of the EnzCheck lipase substrate through an implanted OmFC. The lipase substrate shifts its fluorescence to emission peak 515 nm (green) in the presence of lipases, and we detected the green signals using our photometry system in a temporal manner. Intra-PVH injection of EnzCheck lipase substrate was performed 4 h before placing mice in a temperature-controlled chamber. Cold induced a potent increase in the green signals generated from the lipase substrate, indicating increased lipolysis (Fig. 5A-B). To validate the signals, mice were injected with pan-lipase inhibitor diethylumbelliferyl phosphate (DEUP) via intra-PVT injections to inhibit lipolysis. Cold-induced lipolysis was reduced with the treatment of DEUP compared to vehicle-treated mice (Fig. 5C). These results are consistent with the cold-induced increase in lipolytic markers (Fig. $1A_1$ and A_2), further indicating that cold induces lipolysis in the PVH by increasing cytoplastic

lipases. To examine whether neuronal activity is required for cold-induced lipolysis, in cohort groups of PVH-implanted mice which were treated with the lipase substrate via intra-PVH injections, we performed intra-PVH injections of the MUS and KYN 30 min before placing the mice in a cold chamber. We observed that MUS and KYN inactivation of neurons prevented the cold-induced conversion of the lipase substrate, indicating decreased lipolytic activity (Fig. 5D). These findings suggest that cold induces a rapid neuron activity-dependent lipolytic effect.

Neuronal inactivation prevents cold-induced formation of LDs

To verify our results of LDs detected in the fixed tissues (Fig. 2), we next performed time-lapse photometry monitoring of dynamics of LDs *in vivo* in freely behaving mice. To achieve this goal, we implanted an OmFC cannula in PVH for LD marker BD493 (green) injections and LD monitoring in mice. Matching with the results collected from the fixed sections, cold induced an increase in the intensity of BD493 signals (Fig. 6A and B). This result indicates that cold increases the formation of LDs which could be directly used for lipolysis by releasing fatty acids to mitochondria for β-oxidation. To define a role of neuronal activity in modulating LDs, we performed intra-cannula injections of both MUS and KYN in BD493-injected mice in the PVH. MUS and KYN administration blunted the cold-induced increase in LDs, as cold failed to increase the BD493 signals compared to controls (Fig. 6C).

Discussion

For survival, it is crucial in precisely modulating lipid metabolism in both the peripheral tissues and brain in mammalian animals. Extensively studies have been focused on lipid metabolism in peripheral tissues particularly adipose tissues while little or nothing was known about that in the brain. This was probably in part because of limited techniques. By taking advantage of combined coordinated neurobiology methods and lipid metabolic assays, we provided in this

study the *in vivo* evidence that cold is capable to induce acute neuronal activity-dependent lipid metabolic activities, including lipid peroxidation and mobilization, lipid droplet formation, and lipid lipolysis in the brain. These results fill in a missing but important gap in our understanding of brain region selective lipid metabolism in physiological conditions such as cold applied in this study. Also, our *in vivo* time-lapse fiber photometry approach detecting probe-labelled lipid metabolites would provide an alternative method to evaluate the dynamics of lipid metabolism in live animals. We believe our studies will also be paradigmatic for understanding abnormal lipid metabolism in brain regions modifying metabolism in metabolic disorders such as obesity.

The third ventricle adjacent PVH is a conserved brain region (*Machluf et al., 2011*), composed of different neuronal populations including multiple brain regions-projecting parvocellular neurons and magnocellular neurons. Particularly, PVH plays varied crucial roles in modulating the hypothalamic-pituitary-adrenal (HPA) axis and the hypothalamic-pituitary-thyroid axis (HPT) (*Swanson et al., 1983*). This determines a key role of the PVH in modulating body functions, energy metabolism and glucose homeostasis in health and disease. Our findings in this study show that cold increases the expressions levels of Fos, lipid peroxidation, LDs formation, and lipolytic markers selectively in the PVH. These findings reveal a new role for the PVH in preventing fatty acid toxicity in pathological conditions.

Activated neurons would induce phospholipid peroxidation to release toxic fatty acids. One recent elegant study (*Ioannou et al., 2019*) shows that nearby astrocytes have the capacity to endocytose neuron-released fatty acids (FAs), store them in LDs, and liberate FAs from LDs through lipolytic processes to mitochondria for β-oxidation. Consistently, our *in vivo* data in this study demonstrate that cold-induced lipid peroxidation and lipolysis in the brain are also under the control of neuronal activities. These findings by us and Ioannou *et al*. (2019) suggest that neurons play an important initiation role in inducing lipid metabolism and fatty acid accumulations in the brain in certain physiological and pathological conditions.

Lastly, the brain is highly thermal sensitive (*Brooks, 1983*) and a metabolic organ that intensively produce heat (*Howarth et al., 2012; Lamanna et al., 1980; Yablonskiy et al., 2000*). Brain temperature has recently increasingly drawn attention to both basic and clinical studies in health and disease. Evidence shows that the brain's energy expenditure efficiency largely depends on the temperature (*Yu et al., 2012*), and temperature gradients between different brain regions exist (*Anderson and Moser, 1995; Delgado and Hanai, 1966; Hayward and Baker, 1968; Mcelligott and Melzak, 1967; Moser and Mathiesen, 1996; Thornton, 2003*). We therefore assume that the capacity for the brain to regulate lipid metabolism is of brain-region specificity and depends on the expressions of temperature sensitive lipid lipolytic and thermogenic markers. In this study, we find that PVH is sensitive to cold and participates in the regulation of brain lipid metabolism. Therefore, identifying the genes and brain regions sensitive to ambient temperature, with the approach applied in this study, is thus significant and important in understanding brain metabolism, providing potential targetable sites in the treatment of brain lipid metabolism-associated neurological and metabolic disorders.

Methods

Experimental protocols were approved by the Institutional Animal Care and Use Committees at the Albert Einstein College and conducted following the U.S. National Institutes of Health guidelines for animal research.

Animals

C57/BL6J wild type mice (#000664, Jackson Laboratory) have been described previously and are available from The Jackson Laboratory. Both male and female mice (age 8-12 weeks) were used at the start of experiments. Mice were group-housed 3–5 mice per cage in humidity- and temperature (22–25 °C)-controlled rooms on a 12-hour light:dark cycle (lights on from 8:00 a.m. to 8:00 p.m.) with *ad libitum* access to water and mouse regular chow (#5001, LabDiet). Mice were single-caged after they received viral transductions with or without guide or optic fiber cannula insertion until all the experimental procedures were finished.

Pharmacology

All the chemicals were purchased from Sigma except where noted. For the experiments requiring intra-PVH injections, an injector with 1-mm extension beyond the custom-made optical fiber multiple fluid injection cannula (OmFC) (Doric Lens) implanted over the PVH was attached by polyethylene tubing to a Hamilton syringe. The injection was performed at a speed of 50 nl per min for 4 min using a matched fluid injector consisiting of a 1.25 mm ferrule and a sleeve connector, and the injector was withdrawn 10 min after the final injection. Grip cement (DENTSPLY) was used to anchor the cannula to the skull, and a plug was inserted to keep the cannula from becoming clogged when the injector was not in place. Mice were then returned to the home cage for one week at least before the experiments. The amount for intra-PVH injection was 200 nl of vehicle or chemicals (in μM): 100 BODIPY™ 493/503 (D3922, Invitrogen), 100 BODIPY™ 581/591 C11 (D3861, Invitrogen), 1 MitoSOX™ Mitochondrial Superoxide Indicators (M36005, Invitrogen), 1 EnzChek™ Lipase Substrate 505/515 (E33955, Invitrogen), 100 Diethylumbelliferyl phosphate (D7692, Sigma), and 500 α-Tocopherol (#258024, Sigma); or 200 nl of 250 pmol Muscimol (M1523, Sigma) and 100 mol Kynurenic acid (K3375, Sigma).

Stereotaxic OmFC implantations for intra-PVH injections and photometry.

Following our previously documented protocols (*Chen et al, 2022; Zhang et al., 2020*), mice were anesthetized with 3% isoflurane to induce the anesthesia and with 1.5–2.0% isoflurane to maintain anesthesia during the surgery, and placed in a stereotaxic frame (Kopf Instruments). A small incision was made in the skin of the head, a small hole was drilled on the skull, and mice were implanted with a custome-made optical fiber multiple fluid injection cannula (OmFC) (Doric Lens) over the PVH (coordinates from bregma: AP -0.8 mm, 0.2 mm from midline, DV -4.0 mm). The cannula was fixed to the skull with stainless steel screws and dental cement. After the surgery, all mice received meloxicam (5 mg/kg) and continued to be housed individually. Two weeks after surgery, the mice were briefly anesthetized and inserted with the fluid injector (with 1 mm protrusion) into PVH. For intra-PVH injection, the injector was attached to a Hamilton syringe through a polyethylene tube and the mice received 200 nl of vehicle, chemicals as listed in the Pharmacology section, or viral vectors (AAV_5-CamKII-$GCaMP_{6f}$-WPRE-SV40, addgene#100834, titer, 2.3×10^{13} GC/ml) or chemicals as stated above, at a rate of 50 nl/min.

Micro-punches of hypothalamic nuclei

As described in our previously published studies (*Qi and Yang, 2015; Chen et al, 2022; Zhang et al., 2020*), acute brain slices that include hypothalamic PVH, LH, DMH, VMH, and ARC respectively were prepared. Briefly, mice were first placed in a cold chamber (4 °C) for 30 min or 4-6 h respectively, as described in the text and figure legends. After the cold exposure, mice were deeply anesthetized with isoflurane and decapitated. The mouse brains were dissected rapidly and palced in ice-cold oxygenated (95% O_2 and 5% CO_2) solution containing the following (in mM): 110 choline chloride, 26.2 D-glucose, 2.5 KCl, 1.25 NaH_2PO_4, 2 $CaCl_2$, 7 $MgSO_4$, 11.6 Na-L-ascorbic acid, and 3.1 Na-pyruvate. Coronal brain slices (280 μm thick) were cut with a vibratome (Leica; VT 1200 S) and maintained in an incubation chamber containing artificial cerebrospinal fluids (aCSFs) (in mM): 119 NaCl, 25 $NaHCO_3$, 11 D-glucose, 2.5 KCl, 2.5 $CaCl_2$, 1.3 $MgSO_4$, and 1 NaH_2PO_4. Micro-punches of the PVH, LH, DMH, VMH and ARC were performed using a punch (1.5 mm diameter; Stoelting#57403) or a pipette tip (1.5 mm diameter). Six micro-punches of each region were obtained from each mouse were respectively collected and immediately placed in 200 μl Trizol reagent (Invitrogen) and stored at -80 °C until analysis.

Total RNA extractions and Real-time qPCR (RT-qPCR)

Total RNA was extracted using Trizol reagent (Invitrogen) according to manufacturer's instruction. Briefly, the collected tissues were lysed in 200 μl of Trizol reagent (Invitrogen) and 40 μl of chloroform was added into each tube and subsequently vortexed for 15 s. After incubation for 2 min, centrifuged at 12,000 x g for 10 min (4 °C). The aqueous phase was transferred to fresh tube and equal volume of isopropanol was added. The tube was incubated for 20 min and centrifuged at 12,000 × g for 10 min (4 °C). The RNA pellet was washed with 70% ethanol by vortex and centrifuged at 12,000 x g for 10 min (4 °C). cDNA was synthesized by High-Capacity cDNA Reverse Transcription Kit (Applied Biosystems) following the manufacturer's instructions. Real-time qPCR was performed using QuantStudio 3 instruments (Applied Biosystems). The mixture for qPCR reaction was prepared in a final volume of 20 μl containing 1 μl cDNAs and 10 μl of LightCycler 480 SYBR Green I Master (Roche) in the presence of primers at 500 nM. The specific primer sequences used were the following:

The specific primer sequences used were the following:

ATGL forward, 5′-CCAACACCAGCATCCAGT-3′;

ATGL reverse, 5′-CAGCGGCAGAGTATAGGG-3′;

HSL forward, 5′-CGCCATAGACCCAGAGTT-3′

HSL reverse, 5′-TCCCGTAGGTCATAGGAGAT-3′;

Cidea forward, 5′-TGCTCTTCTGTATCGCCCAGT-3′

Cidea reverse, 5′-GCCGTGTTAAGGAATCTGCTG-3′;

Prdm16 forward, 5′-CCACCAGCGAGGACTTCAC-3′

Prdm16 reverse, 5′-GGAGGACTCTCGTAGCTCGAA-3′;

Ucp2 forward, 5′-CAGAGCACTGTCGAAGCCTA-3′

Ucp2 reverse, 5′-GTATCTTTGATGAGGTCATA-3′;

Actb forward, 5′-GCTGTCCCTGTATGCCTCT-3′

Actb reverse, 5′-GTCTTTACGGATGTCAACG-3′;.

The relative level of expression was calculated using the comparative $2^{-\Delta\Delta CT}$ method.

Two-color two-channel fiber photometry (FP)

Briefly, three excitation wavelengths were used: 560, 505 / 490, and 405 nm. Excitation lights were generated through fiber-coupled two connectorized LEDs (CLED_560 for 560 nm; CLED_505 / 490 for 505 or 490 nm; CLE_405 for 405 nm; Doric Lenses) driven by a four-channel LED driver (LEDD_4; Doric Lenses). The LEDD_4 was controlled by a fiber photometry console (FPC; Doric Lenses) connected to a computer. Excitation lights were passed through two fluorescence MiniCubes (iFMC6_IE(400-410)_E1(460-490)_F1(500-540)_E2(555-570)_F2(580-680)_S)-6 ports with 2 integrated photodetector heads. The single detector measures both signals within the fluorescence detection windows from 500-540 nm and 580-680 nm band. The combined excitation light was sent into a patch cord made of a 400 μm core, 0.48 NA, low-fluorescence optical fiber (Doric Lenses). The patch cord was connected to the implanted OmFC consisting of a 1.25 mm diameter optic fiber via a sleeve (Doric Lenses; Zirconia Sleeve 1.25 mm with black cover; Sleeve_ZR_1.25-BK). Both green and red fluorescence signals were collected through the same patch cord and passed through the same Minicube and focused onto a Fluorescence Detector Head (FDH; Doric Lenses). The photometry experiments were run in a Lock-in mode, and the acquisition rate was set to 12.0 ksps*C controlled by Doric Neuroscience Studio software (Doric Lenses). The FP experiments were performed 5 min after connecting the optic fibers to the animals. We processed the signals using the Doric Neuroscience Studio software (V5.3.3.14) to calculate the normalized fluorescence variation of the images (ΔF/F), and averaged the signals at 1-s bins. To avoid or

minimize bleaching over time, we performed patch cord photobleaching for 12 h before each experiment, reduced the illumination power outputs as much as possible, and recorded the signals for 30 s every 5 min. We used a rotary joint for long-term photometry recordings in freely moving animals.

Immunofluorescence staining

Mice were euthanized and transcardially perfused with 1 x phosphate buffered saline (PBS, pH 7.4) followed by 4% paraformaldehyde in phosphate buffer (PFA, pH 7.2). Mouse brains were removed and post-fixed in 4% PFA overnight. Fixed brains were transferred to 30% sucrose in PBS for cryoprotection. Next, 30 μm coronal sections were cut in a freezing cryostat (Leica). For immunofluorescence, slices were washed three times in 1 x PBS for 10 min each and heat-incubated with target antigen retrieval solution (Invitrogen) for 2 min at 95 °C. And then, the slices were washed three times in 1 x PBS for 10 min each, followed by permeabilization in 1% triton X-100 solution in 1 x PBS for 40 min at room temperature. After blocking for 1 hour at room temperature, the slices were incubated with a mouse Fos antibody (1:150, sc-166940 AF647, Santa Cruz Biotechnologies) for overnight at 4 °C in the dark. The slices were then rinsed three times in 0.1% triton X-100 solution in 1 x PBS for 10 min each. For lipid droplet staining, slices were washed three times in 1 x PBS for 10 min each and then incubated with 1% triton X-100 solution in 1 x PBS for 40 min. After blocking for 1 hour, the slices were stained with 20 μg/mL BODIPY 493/503 (Invitrogen, D3922) for 4 hours at room temperature in the dark. After the incubation, the slices were rinsed three times in 0.1% triton X-100 solution in 1 x PBS for 10 min each. For perilipin-2 and BODIPY 493/503 co-staining, after permeabilization in 1% triton X-100 solution in 1 x PBS for 40 min and blocking for 1 hour at room temperature, the slices were incubated with rabbit perilipin-2 antibody (1:200, CL594-15294, Proteintech) for overnight at 4 °C in the dark. The slices were then washed three times in 0.1% triton X-100 solution in 1x PBS for 10 min and incubated with 20 μg/mL BODIPY 493/503 (Invitrogen, D3922) for 4 hours at room temperature in the dark and then washed three times in 0.1% triton X-100 solution in 1x PBS for 10 min each time. The stained slices were dried and mounted with mounting medium (0100–20, Southern Biotech). Images were taken using the All-in-One Fluorescence Microscope (BZ-X800E Keyence) and analyzed using the BZ-X800 Analyzer (Keyence).

Author contributions: H.Y.M. and Y.Y. conceived, designed, and performed the experiments, analyzed data, and wrote the manuscript. Y.Y.Y. edited the manuscript.

Acknowledgements: We thank all the members of the Yang laboratory for discussion and critical comments on this study. We thank the Doric Lenses for helping us build and adjust the two-channel two-color photometry rig. For the genetically encoded calcium indicator $GCaMP_{6f}$ plasmids, we thank Dr. James M Wilson for depositing the plasmid of pENN-AAV-CamKII-$GCaMP_{6f}$-WPRE-SV40. This work was supported by the NIH (R01 MH109441, R01 DK112759, R01 DK135717, R01 DK134650 to Y.Y.) and Einstein Research Foundation.

Competing interests: Authors declare no competing interests.

Data and materials availability: All data are available in the main text or the supplementary materials.

References

Andersen P, Moser EI (1995) Brain temperature and hippocampal function. *Hippocampus* **5**:491-498.

Andersen M, Tsopanidou A, Radovanovic T, Compere VN, Hauglund N, Nedergarrd M et al. (2023) Using fiber photometry in mice to estimate fluorescent biosensor levels during sleep. *Bio Protoc* **13**:e4734.

Barbalho CA, Nunes-de-Souza R, Canto-de-Souza A (2009) Similar anxiolytic-like effects following intra-amygdala infusions of benzodiazepine receptor agonist and antagonist: evidence for the release of an endogenous benzodiazepine inverse agonist in mice exposed to elevated plus-maze test. *Brain Res* **1267**:65-76.

Bartelt A, Heeren J (2014) Adipose tissue browning and metabolic health. *Nature Reviews Endocrinology* **10**:24-36.

Brooks VB (1983) Study of brain function by local, reversible cooling reviews of physiology, biochemistry and pharmacology. Vol 95 Berlin; Heidelberg: Spring, 1-109.

Chen D, Qi Y, Zhang J, Yang Y (2022) Deconstruction of a hypothalamic astrocyte-white adipocyte sympathetic axis that regulates lipolysis in mice. *Nat Commun* **13**:7536.

Carpentier AC, Blondin DP, Haman F, Richard D (2023) Brown adipose tissue-a translational perspective. *Endocrine Reviews* **44**:143-192.

Farese RV Jr, Walther TC (2009) Lipid droplets finally get a little R-E-S-P-E-C-T. *Cell* **139**:855-860.

Geller S, Arribat Y, Netzahualcoyotzi C, Lagarrigue S, Carneiro L, Zhang L et al. (2019) Tanycytes regulate lipid homeostasis by sensing free fatty acids and signaling to key hypothalamic neuronal populations via FGF21 secretion. *Cell Metab.* **30**:833-844.

Grabner GF, Xie H, Schweiger M, Zechner R (2021) Lipolysis: cellular mechanisms for lipid mobilization from fat stores. *Nat Metab.* **3**:1445-1465.

Guyton AC, Hall JE (2006) Textbook of medical physiology. Philadelphia:Elsevier Saunders.
Delgado JM, Hanai T. 1996. Intracerebral temperatures in free-moving cats. *Am J Physiol*. **211**:755-769.

Hayward JN, Baker MA (1968) Role of cerebral arterial blood in the regulation of brain temperature in the monkey. *Am J Physiol*. **215**:389-403.

Howarth C, Gleeson P, Attwell D (2012) Updated energy budgets for neural computation in the neocortex and cerebellum. *J Cereb Blood Flow Metab*. **32**:1222-132.

Ioannou MS, Jackson J, Shen SH, Chang CL, Weigel AV, Liu H et al. (2019) Neuron-astrocyte metabolic coupling protects against activity-induced fatty acid toxicity. *Cell* **177**:1522-1535.

Kajimura S, Saito M (2014) A new era in brown adipose tissue biology: molecular control of brown fat development and energy homeostasis. *Annu Rev Physiol*. **76**:225-249.

LaManna JC, Rosenthal M, Novack R, Moffett DF, Jobsis FF (1980) Temperature coefficients for the oxidative metabolic responses to electrical stimulation in cerebral cortex.
J Neurochem. **34**:203-209.

Liu L, Zhang K, Sandoval H, Yamamoto S, Jaiswal M, Sanz E et al. (2015) Glial lipid droplets and ROS induced by mitochondrial defects promote neurodegeneration. *Cell* **160**:177-190.

Long AP, Manneschmidt AK, VerBrugge B., Dortch MR, Minkin SC, Prater KE et al. (2012) Lipid droplet De Novo formation and fission are linked to the cell cycle in fission Yeast. *Traffic* **13**:705-714.

Machluf Y, Gutnick A, Levkowitz G (2011) Development of the zebrafish hypothalamus. *Ann NY Acad Sci*. **1220**:93-105.

Mcelligott JG, Melzack R (1967) Localized thermal changes evoked in the brain by visual and auditory stimulation. *Exp Neurol* **17**:293-312.

Moser EI, Mathiesen LI (1996) Relationship between neuronal activity and brain temperature in rats. *Neuroreport* **7**:1876-1880.

Murphy DJ (2001) The biogenesis and functions of lipid bodies in animals, plants and microorganisms. *Prog. Lipid Res*. **40**:325-438.

Olzmann JA, Carvalho P (2019) Dynamics and functions of lipid droplets. *Nat Rev, Mol Cell Biol* **20**:137-155.

Pozo M, Claret M (2018) Hypothalamic control of systemic glucose homeostasis: the pancreas connection. *Trends Endocrinol Metab.* **29**:581-594.

Qi Y, Yang Y. 2015. Hunger states control the directions of synaptic plasticity via switching cell type-specific subunits of NMDA receptors. *J Neurosci*. **35**:13171-13182.

Sanders SK, Shekhar A (1995) Regulation of anxiety by GABAA receptors in the rat amygdala. *Pharmacol Biochem Behav*. **52**:701-706.

Smolic T, Tavcar P, Horvat A, Cerne U, Vasle AH, Tratnjek L *et al.* (2020) Astrocytes in stress accumulate lipid droplets. *Glia* **69**:1540-1562.

Spangenburg EE, Pratt SJP, Wohlers LM, Lovering RM (2011) Use of BODIPY (491/503) to visualize intramuscular lipid droplets in skeletal muscle. Methodology Report. Volume 2011.

Sun F, Zeng J, Jing M, Zhou J, Feng J, Owen SF *et al.* (2018) A genetically encoded fluorescent sensor enables rapid and specific detection of dopamine in flies, fish, and mice. *Cell* **174**:4810496.

Swanson LW, Sawchenko PE (1983) Hypothalamic integration: organization of the paraventricular and supraoptic nuclei. *Annu Rev Neurosci*. **6**:269-324.

Thornton K (2003) The electrophysiological effects of a brain injury on auditory memory functioning. The QEEG correlates of impaired memory. *Arch Clin Neuropsychol*. **18**:363-378.

Wang H, Wang B, Normoyle KP, Jackson K, Spitler K, Sharrock MF et al., 2014. Brain temperature and its fundamental properties: a review for clinical neuroscientists. *Frontiers Neuroscience* **8**:307.

Waterson MJ, Horvath TL (2015) Neuronal regulation of energy homeostasis: beyond the hypothalamus and feeding. *Cell Metab.* **6**:962-970.

Yablonskiy DA, Ackerman JJ, Raichle ME (2000) Coupling between changes in human brain temperature and oxidative metabolism during prolonged visual stimulation. *Proc Natl Acad Sci U S A* **97**:7603-7608.

Yoshida J, Tomonaga S, Ogino Y, Nagasawa M, Kurata K, Furuse M (2012) Intracerebroventricular injection of kynurenic acid attenuates corticotrophin-releasing hormone augmented stress responses in neonatal chicks. *Neurosci*ence **220**:142-148.

Yu Y, Hill AP, Mccormick DA (2012) Warm body temperature facilitates energy efficient cortical action potentials. *PLoS Comput Biol*. **8**:e1002456.

Zhang J, Chen D, Sweeney P, Yang Y (2020) An excitatory ventromedial hypothalamus to paraventricular thalamus circuit that suppresses food intake. *Nat Commun*. **11**:6326.

Figure Legends

Figure 1. Brain region selective responses to cold. Micro-punches of PVH, LH, DMH, VMH, and ARC were made from male mice exposed to a cold chamber for 4-6 h, which were directly used for RT-qPCR of the gene markers of lipolysis and thermogenesis. (A_1-A_5) Group data of the lipolytic marker *ATGL* (A_1) and *HSL* (A_2) as well as thermogenic marker *Ucp2* (A_3), *Cidea* (A_4) and *Prdm16* (A_5) in the PVH. (B_1-B_5) Group data of the lipolytic marker *ATGL* (B_1) and *HSL* (B_2) as well as thermogenic marker *Ucp2* (B_3), *Cidea* (B_4) and *Prdm16* (B_5) in the LH. (C_1-C_5) Group data of the lipolytic marker *ATGL* (C_1) and *HSL* (C_2) as well as thermogenic marker *Ucp2* (C_3), *Cidea* (C_4) and *Prdm16* (C_5) in the DMH. (D_1-D_5) Group data of the lipolytic marker *ATGL* (D_1) and *HSL* (D_2) as well as thermogenic marker *Ucp2* (D_3), *Cidea* (D_4) and *Prdm16* (D_5) in the VMH. (E_1-E_5) Group data of the lipolytic marker *ATGL* (E_1) and *HSL* (E_2) as well as thermogenic marker *Ucp2* (E_3), *Cidea* (E_4) and *Prdm16* (E_5) in the ARC. Data represent mean ± s.e.m. Student *t* tests were performed. *p<0.05. Each dot represents one animal in each group of all the panels.

Figure 2. Cold-induced lipid droplets (LDs) formation in the PVH. Control or cold (30 min~1 h)-challenged mice were perfused and fixed. Mouse brains were sectioned. LDs in the PVH were labelled by BODIPY493 (BD493). (A, B) Representative images of BD493 signals in PVH sections from one control (A) and one cold-challenged mouse (B). (C) Group data of relative BD493-labelled area in PVH in control and cold-challenged mice (n=3 each group). (D-F) Sample images of BD493 (D) and perilipin2 (PLIN2) (E) and overlay (F) signals in the PVH. Data represent mean ± s.e.m. Student *t* tests were performed. **p<0.01. Scale bars, 50 μm for (A, B), and 1 μm for (D-F). PVH, paraventricular of hypothalamus; 3rd V, third ventricle.

Figure 3. Cold increased Fos expressions in the PVH. Control or cold-challenged mouse brains were perfused and fixed and sectioned. Fos in the PVH were labelled using anti-Fos antibodies. (A, B) Representative images of Fos signals in PVH from one control (A) and one cold-challenged mouse (B). (C) Group data of Fos-positive cells in PVH in control and cold-challenged mice (n=3 each group). Data represent mean ± s.e.m. Student *t* tests were performed. **p<0.01. Scale bars, 50 μm for (A, B). PVH, paraventricular of hypothalamus; 3rd V, third ventricle.

Figure 4. Cold-induced neuronal activity-dependent lipid peroxidation in the PVH in freely behaving mice. Mice were injected with the lipid peroxidation indicator BD-C11 in the PVH via the implanted OmFC cannula 4 h before placing them in a temperature-controlled chamber. Two-color fiber photometry was used for time-lapse monitoring of BD-C11 convertion via the optic fiber of the OmFC. (A) Representative traces of real-time photometry monitoring of red and green signals simultaneously. (B-D) Group data of relative BD-C11 ratio to baseline in mice treated with vehicle (B, n=6), α-TP (C, n= 4), and KYN+MUS (D, n=4). Data represent mean ± s.e.m. Student *t* tests were performed.

Figure 5. Cold-induced neuronal activity-dependent lipid lipolysis. Mice were injected with the lipase substrate in the PVH via the implanted OmFC cannula 4 h before placing them in a temperature-controlled chamber. Two-color fiber photometry was used for time-lapse monitoring of lipase substrate convertion via the optic fiber of the OmFC. (A) Representative traces of real-time photometry monitoring of green signals. (B-D) Group data of lipase substrate convertion in mice treated with vehicle (B, n=4), α-TP (C, n= 4), and KYN+MUS (D, n=4). Data represent mean ± s.e.m. Student *t* tests were performed.

Figure 6. Cold-induced neuronal activity-dependent formation of LDs. Mice were injected with the LD marker BODIPY493 in the PVH via the OmFC cannula 4 h before placing them in a temperature-controlled chamber. Fiber photometry was used for time-lapse monitoring of BODIPY493 signals via the optic fiber of the OmFC. (A) Representative traces of real-time photometry monitoring of BODIPY493 signals. (B-D) Group data of BODIPY493 in mice treated with vehicle (B, n=4), α-TP (C, n= 4), and KYN+MUS (D, n=6). Data represent mean ± s.e.m. Student *t* tests were performed.

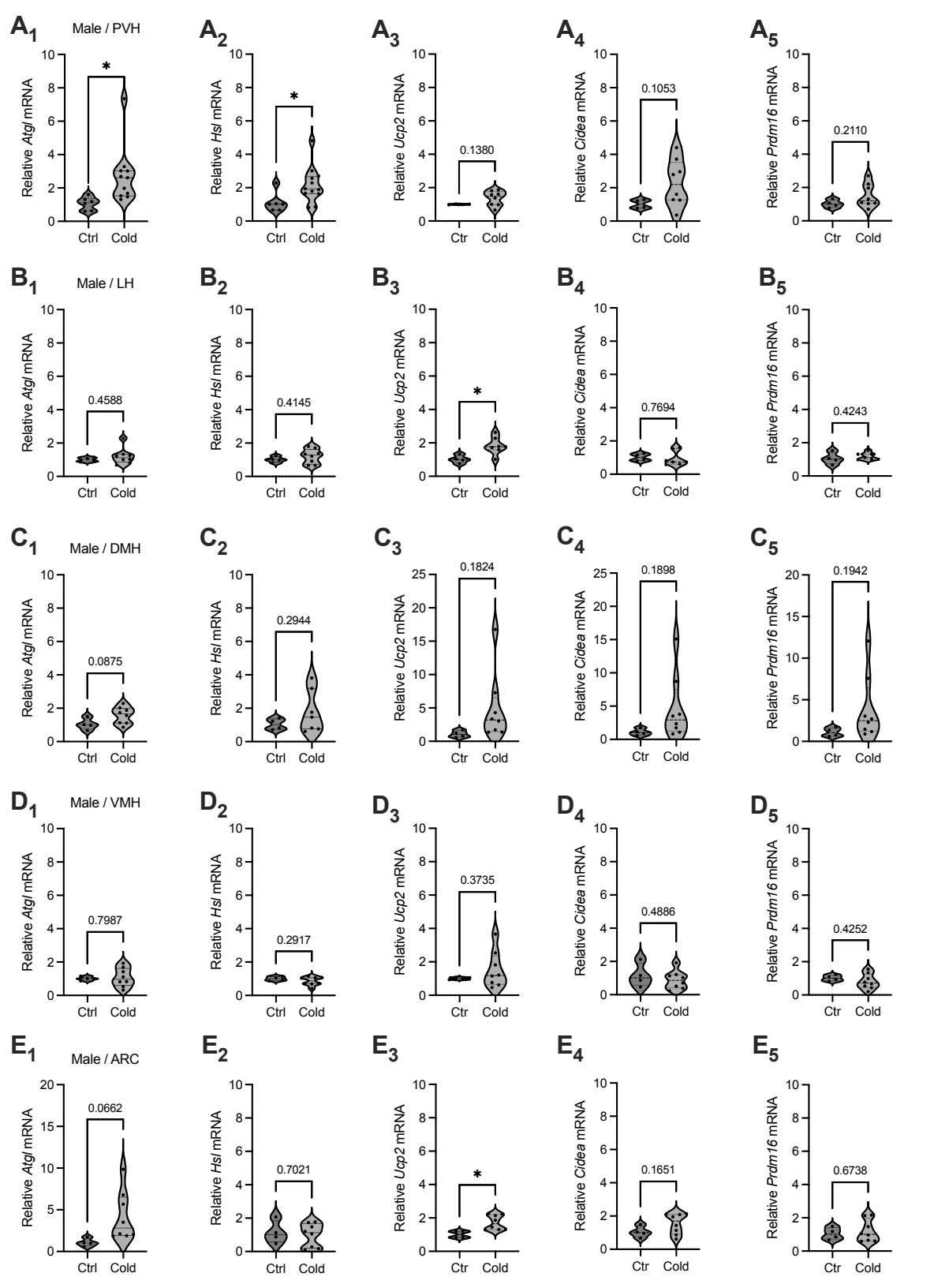
A1
Male / PVH
Relative Atgl mRNA
*
Ctrl
Cold
A2
Relative Hsl mRNA
*
Ctrl
Cold
A3
Relative Ucp2 mRNA
0.1380
Ctr
Cold
A4
Relative Cidea mRNA
0.1053
Ctr
Cold
A5
Relative Prdm16 mRNA
0.2110
Ctr
Cold
B1
Male / LH
Relative Atgl mRNA
0.4588
Ctrl
Cold
B2
Relative Hsl mRNA
0.4145
Ctrl
Cold
B3
Relative Ucp2 mRNA
*
Ctr
Cold
B4
Relative Cidea mRNA
0.7694
Ctr
Cold
B5
Relative Prdm16 mRNA
0.4243
Ctr
Cold
C1
Male / DMH
Relative Atgl mRNA
0.0875
Ctrl
Cold
C2
Relative Hsl mRNA
0.2944
Ctrl
Cold
C3
Relative Ucp2 mRNA
0.1824
Ctr
Cold
C4
Relative Cidea mRNA
0.1898
Ctr
Cold
C5
Relative Prdm16 mRNA
0.1942
Ctr
Cold
D1
Male / VMH
Relative Atgl mRNA
0.7987
Ctrl
Cold
D2
Relative Hsl mRNA
0.2917
Ctrl
Cold
D3
Relative Ucp2 mRNA
0.3735
Ctr
Cold
D4
Relative Cidea mRNA
0.4886
Ctr
Cold
D5
Relative Prdm16 mRNA
0.4252
Ctr
Cold
E1
Male / ARC
Relative Atgl mRNA
0.0662
Ctrl
Cold
E2
Relative Hsl mRNA
0.7021
Ctrl
Cold
E3
Relative Ucp2 mRNA
*
Ctr
Cold
E4
Relative Cidea mRNA
0.1651
Ctr
Cold
E5
Relative Prdm16 mRNA
0.6738
Ctr
Cold

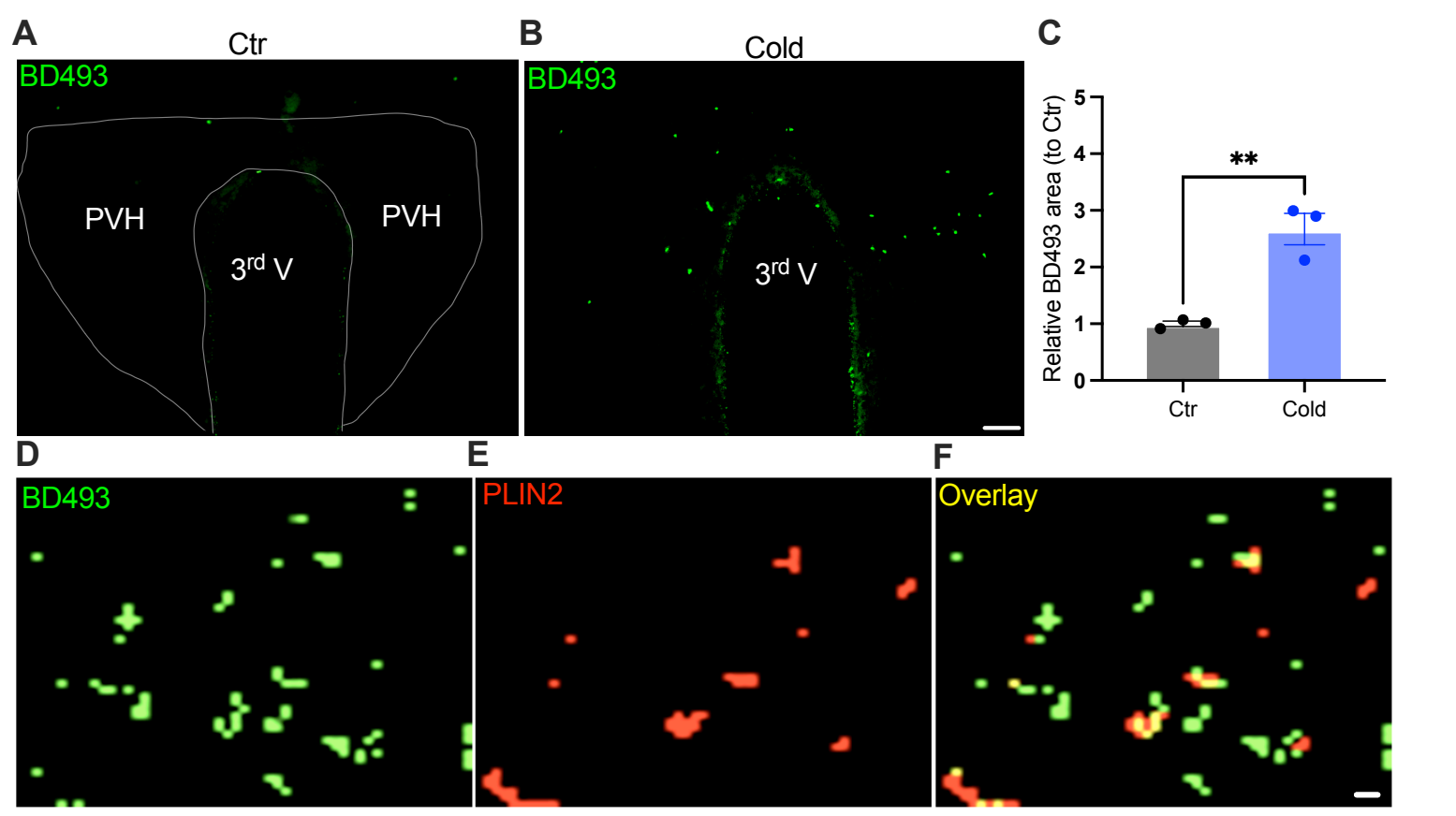
A
Ctr
BD493
PVH
PVH
3rd V
B
Cold
BD493
3rd V
C
Relative BD493 area (to Ctr)
0
1
2
3
4
5
**
Ctr
Cold
D
BD493
E
PLIN2
F
Overlay

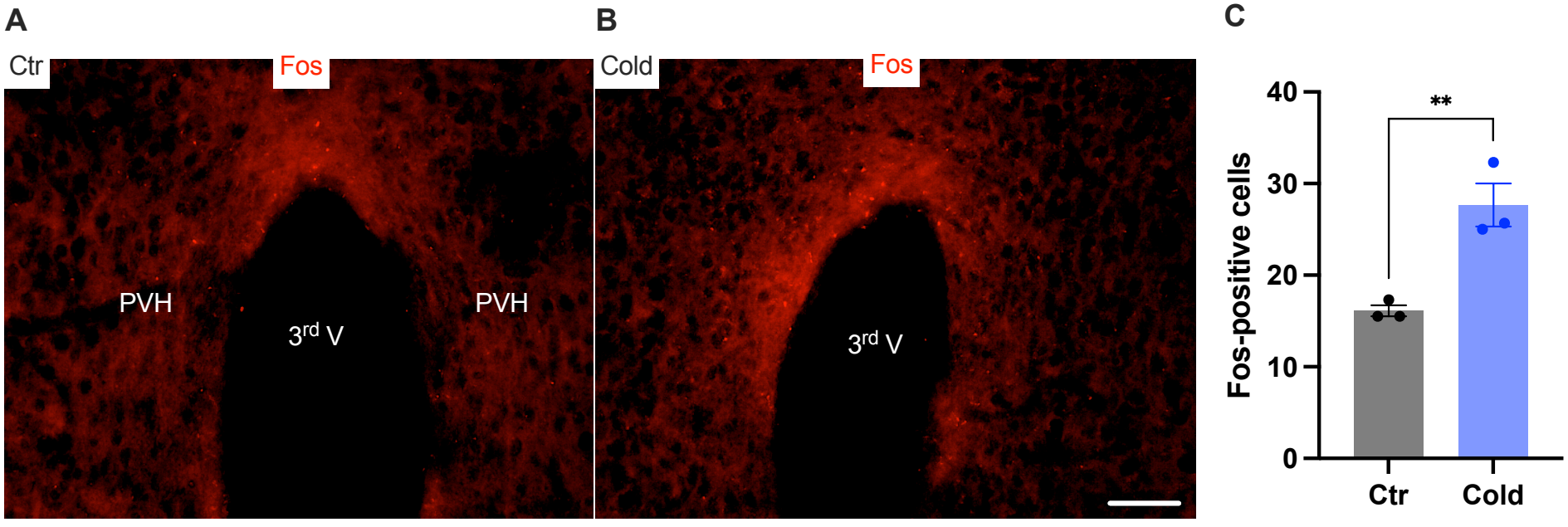
A
Ctr
Fos
PVH
3rd V
PVH
B
Cold
Fos
3rd V
C
Fos-positive cells
40
30
20
10
0
**
Ctr
Cold

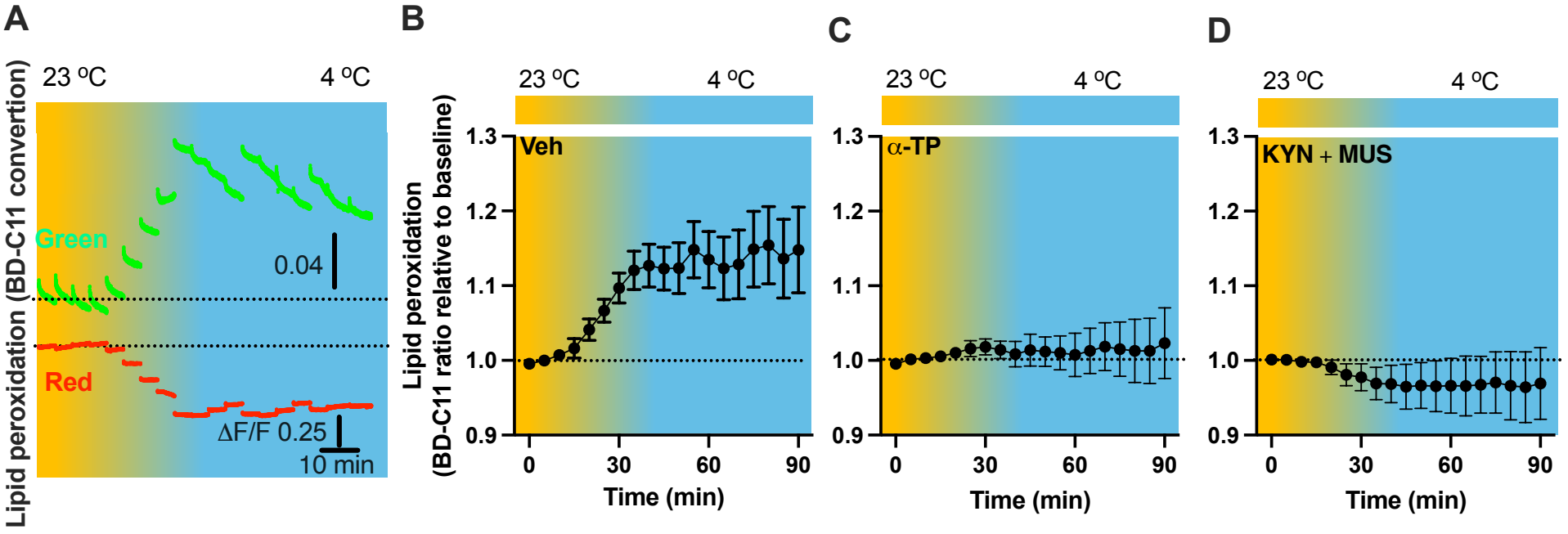
A
23 ºC
4 ºC
Green
0.04
Red
ΔF/F 0.25
10 min
Lipid peroxidation (BD-C11 convertion)
B
23 ºC
4 ºC
Veh
Lipid peroxidation
(BD-C11 ratio relative to baseline)
1.3
1.2
1.1
1.0
0.9
0
30
60
90
Time (min)
C
23 ºC
4 ºC
α-TP
1.3
1.2
1.1
1.0
0.9
0
30
60
90
Time (min)
D
23 ºC
4 ºC
KYN + MUS
1.3
1.2
1.1
1.0
0.9
0
30
60
90
Time (min)

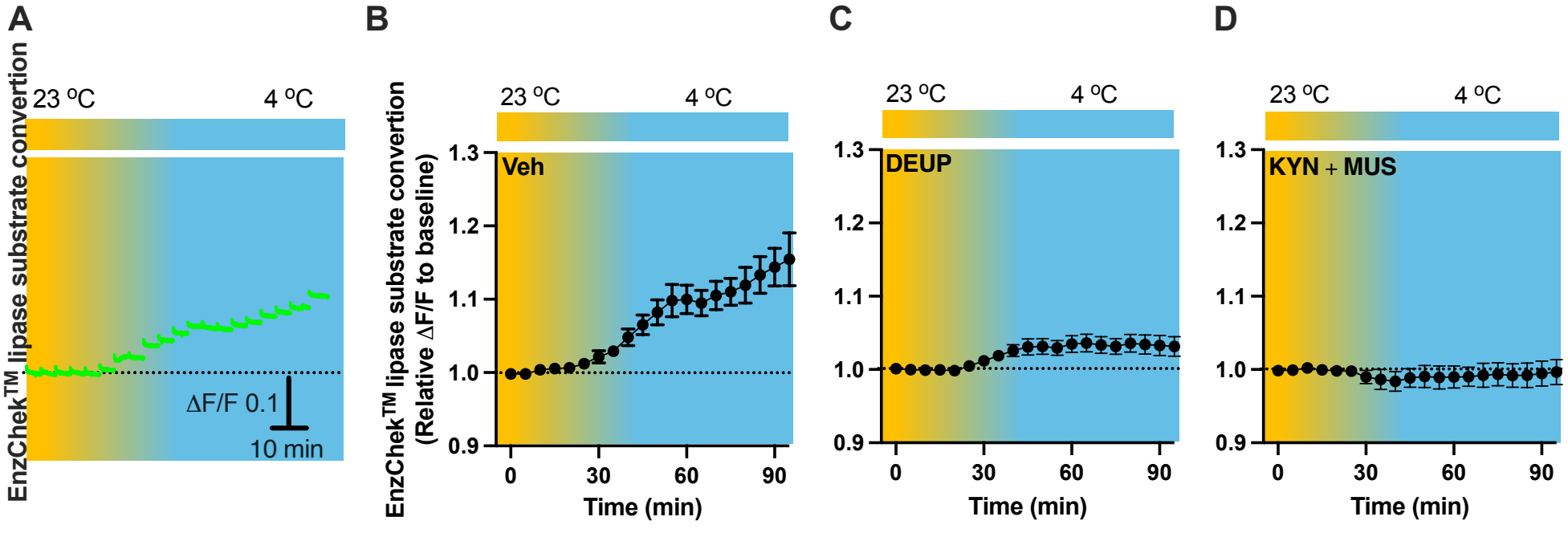
A
B
C
D
23 ºC
4 ºC
EnzChek™ lipase substrate convertion
ΔF/F 0.1
10 min
EnzChek™ lipase substrate convertion
(Relative ΔF/F to baseline)
Veh
DEUP
KYN + MUS
1.3
1.2
1.1
1.0
0.9
0
30
60
90
Time (min)

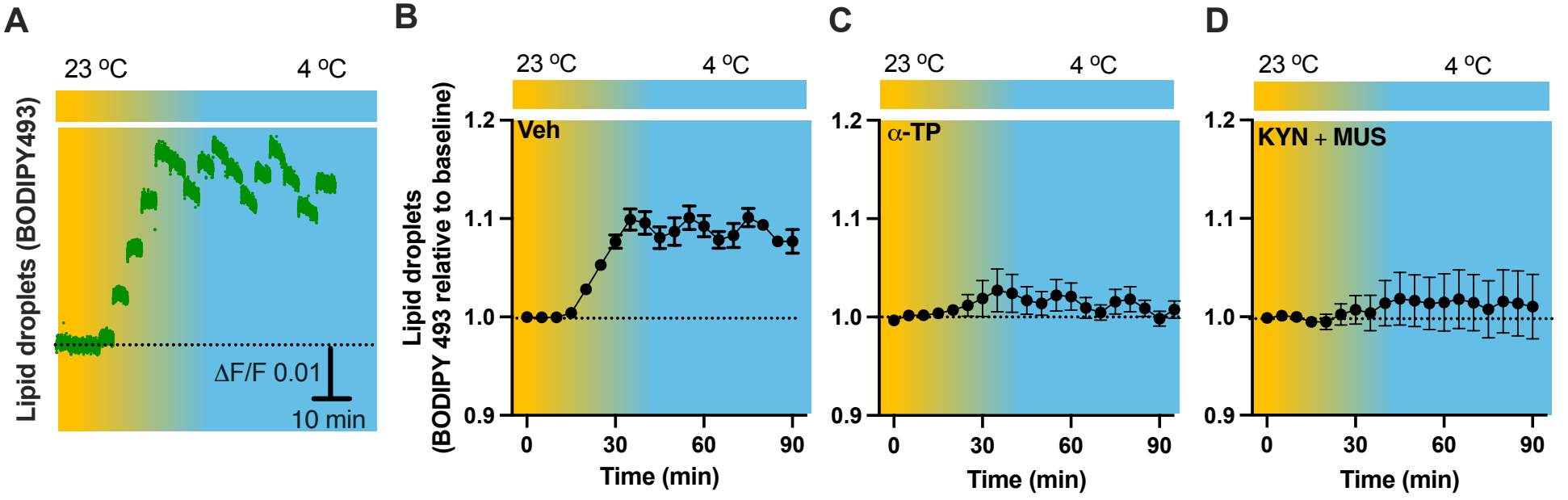
A
23 ºC
4 ºC
Lipid droplets (BODIPY493)
ΔF/F 0.01
10 min
B
23 ºC
4 ºC
Veh
Lipid droplets
(BODIPY 493 relative to baseline)
1.2
1.1
1.0
0.9
0
30
60
90
Time (min)
C
23 ºC
4 ºC
α-TP
1.2
1.1
1.0
0.9
0
30
60
90
Time (min)
D
23 ºC
4 ºC
KYN + MUS
1.2
1.1
1.0
0.9
0
30
60
90
Time (min)